Clutter suppression using Thresholded Reciprocal Filter in OFDM radar

ANDREA QUIRINI
Student Member IEEE, Sapienza University of Rome

FABIOLA COLONE
Senior Member IEEE, Sapienza University of Rome

PIERFRANCESCO LOMBARDO
Senior Member IEEE, Sapienza University of Rome

Abstract — Thresholded reciprocal filtering (TRF) techniques have been proposed as supervision strategies for reciprocal filtering (RF) in order to address the challenges posed by the unique characteristics of orthogonal frequency-division multiplexing (OFDM) waveforms when used for radar. These techniques are known to provide a larger flexibility for the signal processing scheme at the range compression stage by enabling the possibility to operate on signal fragments of arbitrary length, while simultaneously retaining the RF's benefits in terms of point-like target response. In this paper we extend the study of TRF techniques by presenting a theoretical analysis of their impact on the clutter suppression capability of the system. To this end, we firstly characterize the theoretical performance of the TRF techniques in terms of residual clutter power obtained at the output range-Doppler map. The derived analytical expressions further allow us to introduce optimized variants of the TRF, that are able to maximize the performance metrics. An extensive simulation-based validation shows that the proposed solutions outperform traditional methods, especially in low to moderate clutter-to-noise conditions. Moreover, the assessment of the proposed technique against an experimental dataset allows us to validate the practical effectiveness of the TRF approach.

Index Terms — clutter cancellation, OFDM radar, supervised reciprocal filter, passive radar

I. INTRODUCTION

Encouraged by recent advancements in joint radar and communication (JRC), [1]-[3] as well as passive radar (PR) technologies, [5]-[16], orthogonal frequency-division multiplexing (OFDM) radar systems have gained increasing attention within the radar research community.

On one hand, the JRC paradigm introduces an effective approach to address the growing congestion within the radiofrequency spectrum by enabling coexistence between radar and communication systems. This concept finds relevance in applications involving multiple users, such as autonomous drivingor smart indoor environments. Nevertheless, designing a JRC system requires careful design of the waveform jointly exploited by the radar and the communications subsystems. In this perspective, OFDM-modulated signals have emerged as promising candidates.

On the other hand, the concept of exploiting existing transmitters from communication systems as radar illuminators of opportunity has gained substantial attention in the last few decades since it enables cost-effective radar solutions, suitable for various surveillance and short-range monitoring applications. Several studies have explored the feasibility of passive radar based on digital audio broadcasting (DAB [8][9]), digital video broadcasting - terrestrial (DVB-T [9][10][11]), or transmitters used in metropolitan and local area networking (e.g., Wi-Fi [12][13], LTE [14][15], 5G [16]).

However, the use of OFDM-modulated signals for radar purposes introduces issues that have to be carefully considered [6][10][17][18]. As is well known, OFDM waveforms include several structures (e.g., cyclic prefixes, pilot tones or null carriers), which are typically embedded within these waveforms to counter inter-symbol interference, achieve signal synchronization and channel equalization in communication systems. These periodical structures are especially harmful for radar purposes, as they induce undesired side-peaks within the cross-ambiguity function (CAF), which can mask the echoes of targets with low radar cross-section. Moreover, the time-varying nature associated to the information content of the employed OFDM waveforms also jeopardizes clutter cancellation, as the unpredictable changes in the waveform cause subsequent observations of the stationary scene to decorrelate.

Recent works have addressed these issues by introducing signal processing strategies based on the use of a reciprocal filter (RF) at the range compression stage [7][11][19]-[21]. In fact, the RF inherently equalizes the spectral modulation induced by the waveform characteristics thus yielding an ideal sinc-shaped response to a point-like target echo. Also, this response remains stable across consecutive observations regardless of the time-varying data content. This in turn enables perfect clutter suppression through conventional low-complexity approaches, such as the non-adaptive single canceller (SC) [22].

Specifically, the signal processing architectures proposed in [19]-[21] operate by (i) dividing the reference and surveillance signals into batches equal to OFDM symbols and removing the cyclic prefix, (ii) applying the RF on a batch-by-batch basis to obtain range compressed data, (iii) performing clutter cancellation with a SC, (iv) evaluating the final range-Doppler map by applying an FFT across consecutive batches. The adopted OFDM signal fragmentation determines remarkable performance for the RF in terms of clutter removal and sidelobes control with only a limited signal-to-noise (SNR) loss with respect to the conventional matched filter (MF).

In contrast, not all the above characteristics are guaranteed when applying the RF over batches not coinciding with OFDM symbols. Nevertheless, the possibility to operate with arbitrarily fragmented signals would provide the radar designer with additional design flexibility in order to be effective in different scenarios:

1. As known, the suboptimal batching strategy neglects the target echo phase variation within each batch. This results in a velocity-dependent SNR loss, since the

entity of the phase shift depends on the bistatic velocity of the target. This suggests using sub-symbol batches, especially when dealing with fast-moving targets.

2. The frequency-domain implementation of range compression also introduces an SNR loss, since a linear correlation is approximated by a circular correlation. The resulting SNR loss depends on the target bistatic range, and can be mitigated by using super-symbol batches, which are more robust to border effects.
3. The equivalent pulse repetition time (PRT) is equal to the duration of the adopted batches. Therefore, decoupling the batch duration from the OFDM symbol duration also allows to select the desired pulse repetition frequency (PRF), which is crucial for unambiguous target detection.
4. Practical implementation, especially on resource-constrained platforms like field programmable gate arrays (FPGAs), benefits from the flexibility enabled by arbitrary signal fragmentation. For instance, using batches shorter than the OFDM symbols may become a necessity when dealing with limited memory resources.

Driven by the potential of arbitrary fragmentation, the application of the RF-based processing on batches of arbitrary duration has been considered in [23]. Therein, it was demonstrated that applying a conventional RF to non-OFDM-fragmented signals results in enormous SNR losses, which depend on the statistical properties of the received signals. Specifically, when the batch does not correspond to the OFDM symbol, its samples are not exclusively drawn from the OFDM constellation and can assume any random value. This is especially problematic when inverting the reference signal spectrum to implement a RF, since it may introduce spikes amplifying the noise power level.

To enable the use of arbitrary fragmentations in conjunction with RF, supervised versions of the RF were introduced in [23], denoted as thresholded reciprocal filter (TRF). The proposed approaches proved effective in avoiding the noise boosting effect while preserving the RF's improved point-like target response.

However, [23] does not consider the impact of the TRF techniques on the clutter suppression capability, which is yet to be explored. In fact, since the supervision strategy relies on the actual values of the signal spectrum at each batch, it partially restores the data-dependent characteristic for the point-like target response. As a consequence, it is expected that the use of TRF at the range compression stage might have a non-negligible impact on the clutter cancellation stage, especially if a low-complexity approach has to be exploited such as the SC. Some preliminary results along this line have been reported in [24]. However, these initial findings lack the theoretical framework needed to assess the clutter suppression capabilities of the TRFs.

Specifically, the novel contributions of this paper can be summarized as follows.

1. The clutter suppression capabilities of a signal processing architecture based on the cascade of a TRF-based range compression and a SC are theoretically assessed. This study not only complements the analysis reported in [23] and extends the qualitative study in [24], but also allows to properly select the TRF parameters in order to identify a suitable trade-off between the clutter cancellation capability and the SNR loss limitation.
2. The availability of closed-form expressions for the observed performance metrics allows us to derive optimized variants of the TRF techniques, in which the parameters are evaluated to optimize different objective functions, namely the SNR, the clutter-to-noise ratio (CNR) and the signal-to-clutter-and-noise ratio (SCNR), respectively.
3. This paper also reports an extensive validation of the performance of different TRF techniques through testing not only against simulated data as in [24], but also against experimental data. This allows to demonstrate the advantages of the proposed solutions in practical cases.

This paper is outlined as follows. In Section II, we introduce the adopted processing scheme based on alternative range compression filters, applied against both OFDM-fragmented and arbitrarily fragmented signals. In Section III, the clutter suppression performance of the cascade of MF/RF/TRF and SC are theoretically assessed and then validated via simulated analysis. In Section IV, the TRF parameters are optimized according to different metrics, and the performance of the optimized TRFs are compared to that of the TRFs introduced in [23]. In Section V, we test the different TRF supervision techniques on synthetic data, considering a DVB-T-based PR. The TRFs are also validated against an experimental dataset in Section VI. Lastly, Section VII offers concluding remarks.

II. SIGNAL PROCESSING SCHEME AND RANGE COMPRESSION STRATEGY

In this paper we consider the signal processing scheme depicted in Figure 1 that was shown to be an effective solution in different OFDM radar applications, especially when designing systems with limited complexity [19]-[21].

The considered architecture encompasses a batching stage where the digitized received signals are first fragmented into batches of assigned length. The fragmented reference and surveillance signals are arranged in bi-dimensional sequences, namely $r[l,m]$ and $s[l,m]$ ($l = 0,\dots L-1, m = 0,\dots M-1$), being L the batch length and M the number of batches included in the coherent

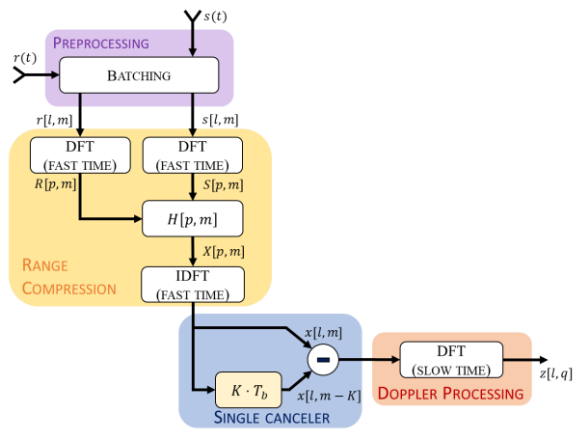

Figure 1: Sketch of the adopted processing architecture.

processing interval (CPI), while l and m represent the fast-time and slow-time indices, respectively.

Then a range compression stage is applied on a batch-by-batch basis, [6][25]. It is performed in the frequency domain, by computing the DFT of the surveillance signal at the m-th batch, namely $S[p,m]$, and evaluating:

$$x[l,m] = \frac{1}{L}\sum_{p=0}^{L-1} S[p,m]H[p,m]e^{\frac{j2\pi pl}{L}}. \quad (1)$$

where $H[p,m]$ is the adopted range compression filter, which might take different forms as discussed later in this section. The range-compressed sequence is fed to the clutter suppression stage, which is based on a single-pulse MTI canceler with a K-taps delay:

$$x_C[l,m] = x[l,m] - x[l,m-K] \quad (2)$$

Finally a discrete Fourier transform (DFT) is performed across batches to obtain the final range-Doppler map:

$$z[l,q] = \sum_{m=0}^{M-1} x_C[l,m]e^{-\frac{j2\pi mq}{M}} \quad (3)$$

Different combinations of batching strategies and range compression filters can be adopted within the architecture in Figure 1 depending on the considered scenario.

OFDM fragmentation: when an OFDM fragmentation is used, signals are fragmented into individual OFDM symbols. The signal batches feeding the range compression stage are obtained by removing the cyclic prefix (CP) from each OFDM symbol. Consequently, the DFT evaluated over the useful OFDM symbol portion of duration T_U takes values out of the adopted modulation constellation [11][19][20].

With this batching strategy, two range compression filters have been considered:

the conventional matched filter (MF):

$$H[p,m] = R^*[p,m] \quad (p = 0,\dots,L-1) \quad (4)$$

the reciprocal filter (RF):

$$H[p,m] = \frac{1}{R[p,m]} \quad (p = 0,\dots,L-1) \quad (5)$$

where $R[p,m]$ is the DFT of the reference signal at the m-th batch. As is well known, the MF allows to maximize the output SNR. In contrast, the RF has been shown to provide a more controlled point-like target response in terms of both stability across time and sidelobe level [19][20]. When an OFDM fragmentation is adopted, these advantages of the RF with respect to the MF are obtained at the price of a limited loss in terms of SNR, which depends on the adopted modulation constellation but is typically below 4-5 dB.

Non-OFDM fragmentation: in this case the batches length L is arbitrarily selected in order to meet requirements related to the range/Doppler region of interest, the presence of Doppler ambiguities, the computational resources, as briefly discussed in the introduction. In such condition, there is no need to identify the start of the OFDM frame or to remove the cyclic prefix, thus further symplifying the batching stage [23].

With this batching strategy, the MF shows identical characteristics as for an OFDM fragmentation: it achieves optimal SNR performance while still suffering from high sidelobes, presence of side-peaks, and large temporal variability in the filter response. The RF is still able to mitigate these undesired characteristics of the MF but at the price of large SNR loss, typically higher than 10 dB [23]. This is due to the fact that, with a non-OFDM fragmentation, the DFT of the surveillance and the reference signals are evaluated over batches that might be shorter or longer than the useful OFDM symbol so that the output takes values not limited to the constellation symbols that can be rather modeled as zero-mean complex gaussian random variables. Consequently there is a non negligible probability for $R[p,m]$ to take very low values that in turn are responsible of a noise boosting effect when used to compute the RF.

Therefore, supervised versions of the RF have been introduced to mitigate this loss the good characteristics of the RF [23]. The idea behind the thresholded RF (TRF) is to supervise the minimum value of the reference signal power spectrum $|R[p,m]|^2$ before the RF is computed. This prevents the occurrence of spikes in the amplitude response $|H[p,m]|$ of the range compression filter. Specifically, the TRF is evaluated as:

$$H[p,m] = \begin{cases} \dfrac{1}{R[p,m]} & |R[p,m]|^2 > x_0 \\ \alpha\, e^{-j\angle R[p,m]}, & |R[p,m]|^2 \le x_0 \end{cases}. \quad (6)$$

where

- x_0 is the threshold and can be set to obtain a good trade-off between output SNR and filter response characteristics, and
- α is constant that defines the particular TRF technique; specifically, three distinct TRF approaches where introduced in [23] based on the following choices of this parameter:
- TRF-Zeros (TRF-Z) – the filter samples triggering the threshold are replaced with zeros ($\alpha = 0$);
- TRF-Mean (TRF-M) – the filter samples triggering the threshold are replaced with the mean spectral amplitude level ($\alpha = 1/\sqrt{E\{|R[p,m]|^2\}} = 1/\sqrt{L\sigma_r^2}$).
- TRF-Saturated (TRF-S) – the filter samples triggering the threshold are replaced with the adopted threshold x_0 ($\alpha = 1/\sqrt{x_0}$).

All the above combinations of batching strategies and range compression filters have been extensively investigated in [23] in terms of achievable SNR and sidelobes characteristics for the resulting response to a point-like target. In particular, the advantages provided by RF based approaches have been compared with the SNR loss that has to be accepted:

$$\Delta_{SNR} = \frac{SNR_{max}}{SNR} \quad (7)$$

and this is evaluated with respect to the maximum SNR achieved with the optimum cross-ambiguity function (CAF) between the surveillance signal and the reference signal for a given CPI, i.e. $SNR_{max} = SNR_{in}\, N$, being N the total number of samples in the CPI.

For a given fragmentation strategy and range compression filter, the above loss is the result of several loss factors, all characterized by the authors in [23]:

- Cyclic Correlation Loss (ρ_{CC}): Performing range compression in the frequency domain implies implementing a circular correlation instead of a linear one. This yields an SNR loss, denoted as ρ_{CC}, increasing with the target's bistatic range. Thanks to the presence of a CP at each OFDM symbol, the OFDM fragmentation strategy prevents this loss for targets within the bistatic range $R_G = c \cdot T_G$, where T_G is the CP duration. On the other hand, with a non-OFDM fragmentation, this loss can be mitigated up to the desired level by increasing the batch duration.
- Doppler-Induced Phase Variation Loss (ρ_{DOP}): The adopted batching strategy inherently neglects the Doppler-induced phase variation within each batch. This introduces an additional SNR loss increasing with the target's bistatic velocity. This loss can be mitigated only with a non-OFDM fragmentation by employing shorter batches.
- CP Loss (ρ_{CP}): this loss is only present with the OFDM-fragmentation since this batching strategy removes the CP before range compression, which results in an additional SNR loss linearly increasing with the CP duration.
- Filter mismatch Loss (ρ_{RC}): Lastly, the advantages of the RF-based range compression come at the cost of mismatching the range compression filter, which results in an additional SNR loss. Its entity depends on both the fragmentation strategy and the range compression filters and it has been theoretically evaluated in [23] for all the approaches described previously. The results are summarized in the second column of Table I. In this table M_C and c_m $(m = 0, \dots, M-1)$ are the size and symbols of the adopted modulation constellation whereas $t = x_0/L\sigma_r^2$ is the normalized threshold used for the supervised RF approaches. Furthermore, $E_1(t)$ denotes the exponential integral function, while erf $(\cdot)$ denotes the error function. We recall that the reported formulas are exact in the OFDM-fragmented case, whereas they are approximate expressions in the non-OFDM-fragmented case since they rely on an exponential distribution model, which might not necessarily be tight. As previously mentioned, with an OFDM fragmentation, the RF yields a limited ρ_{RC} loss even for large constellations (0 dB for QAM, 2.76 dB with 16-QAM and 4.29 dB with 64-QAM). In contrast, when a conventional RF is applied to non-OFDM-fragmented signals, an unacceptable loss occurs. Such loss can be mitigated by exploiting the supervised approaches and carefully selecting the adopted threshold.

With the aim to compare the Δ_{SNR} obtained with different fragmentation strategies and range compression filters, we conducted a simulated analysis considering the case study of a radar exploiting a 64-QAM-modulated OFDM waveform. In the considered scenario, the cyclic prefix has been set to $T_{CP} = T_U/4$, resulting in an overall duration of the OFDM symbol $T_{OFDM} = T_U + T_{CP} = 1120\ \mu s$, with $T_U = 896\ \mu s$. The carrier frequency has been set to $f_C = 690\ MHz$ while the number of sub-carriers is $N_c = 8192$. We assume to operate over 512 OFDM symbols of $(1 + 1/4)N_c = 10240$ samples each, which corresponds to a CPI duration of about 0.57 s. Thermal noise has been simulated as complex Gaussian random variable $(0, \sigma_N^2)$, and its power level has been deliberately set to unity. We considered a point-like scatterer with an input SNR equal to $SNR_{in} = 0\ dB$. For such a target the optimum CAF would provide a $SNR_{max} = 66.23dB$ after range compression and Doppler processing.

The scatterer is located at zero range and zero Doppler so that it is not affected by ρ_{CC} and ρ_{DOP} losses. In contrast, in such condition, the loss factors affecting the Δ_{SNR} are the ρ_{CP} and the ρ_{RC}, which are peculiar characteristics of the fragmentation strategy and range compression filter. Therefore the Δ_{SNR} metric was evaluated by measuring the loss at the output of the range compression stage.

Figure 2 shows the Δ_{SNR} loss as a function of the normalized threshold t, obtained using MF, RF and TRF, considering both OFDM-fragmented and arbitrarily fragmented signals with super-symbol batches of duration $T_b = 4 \cdot T_{OFDM}$. The theoretical predictions and the simulated values are respectively represented by the solid lines and the markers. The following observations are in order.

- The performances of MF and RF are independent of the normalized threshold, so they appear as horizontal lines.
- As expected, the approach based on MF + OFDM fragmentation is only affected by the ρ_{CP} loss since $\rho_{RC} = 1$. Having assumed a CP of 1/4, $\rho_{CP} = 10\log_{10}(1 + 1/4) = 0.9691\ dB$.
- Conversely, the approach based on MF + non-OFDM-fragmentation attains the maximum SNR, as predicted by theory.
- The RF + OFDM-fragmentation strategy undergoes an additional loss ρ_{RF} compared to the MF + OFDM-fragmentation one, due to the RF mismatch. Having used a 64-QAM modulation constellation, the RF experiences a loss of $\rho_{RF} = 4.29\ dB$, as predicted by theory.
- The SNR loss experienced by the RF becomes theoretically infinite when applied to non-OFDM-fragmented signals, since the values of the reference

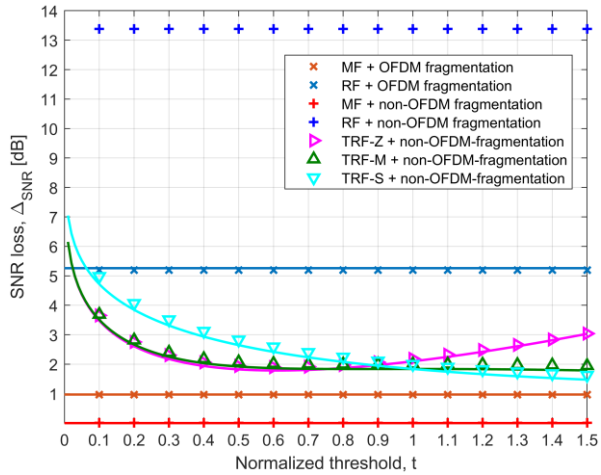

Figure 2: SNR loss obtained using MF, RF and TRF as a function of the normalized threshold t, considering both OFDM-fragmented and arbitrarily fragmented signals.

signal power spectrum samples can eventually reach zero. In practice, simulated results based on limited signal fragments show a highly variable loss which changes from batch to batch. In Figure 2, the RF + non-OFDM-fragmentation approach undergoes a substantial loss of $\Delta_{SNR} \approx 13\,dB$, making it impractical in any application.

- All the TRF techniques recover the SNR loss observed in the RF + non-OFDM fragmentation, enabling the use of a supervised RF on non-OFDM signal fragments. Moreover, increasing the value of t generally results in lower values of Δ_{SNR}. As also discussed in [23], this is not the case for the TRF-Z, since forcing many zero values in the filter spectrum results in the attenuation of the useful signal component also.

The analysis reported above allowed us to recall the benefits of the TRFs in terms of SNR losses as extensively demonstrated in previous papers [23][24]. Basically, such approaches allow to largely recover the loss of a RF when operating with a non-OFDM fragmentation and, in turn, to get advantage of the RF properties together with the benefits of a flexible fragmentation as illustrated in the introduction. In the following, the analysis is extended to investigate the impact that such approaches have on clutter cancellation.

III. IMPACT OF SUPERVISED RECIPROCAL FILTER ON CLUTTER SUPPRESSION

The processing scheme in Figure 1 was shown to be very effective particularly when operating with a RF based compression strategy [19]-[21]. In fact, since the RF yields an ideal sinc-shaped time-invariant response to a point-like target echo regardless of the time-varying data content, its application potentially enables a theoretically perfect clutter suppression for stationary clutter, even operating with a low-complexity non-adaptive SC [20][21].

However, since the supervision strategy relies on the actual values of the signal spectrum at each batch, the application of a TRF partially restores the data-dependent characteristic for the response to a point-like target. As a consequence, it is expected that the use of TRF at the range compression stage might have a non-negligible impact on the clutter cancellation based on the SC.

Therefore, in this section we investigate the performance of the signal processing scheme in Figure 1 in terms of clutter cancellation capability when different combinations are used of range compression techniques and fragmentation strategies.

To this aim, we define the output SCNR as

$$SCNR = \frac{P_T}{P_C + P_N} = SNR\,\frac{1}{CNR + 1} \tag{8}$$

where:

- $P_T = \left|E\left\{z^{(T)}[l_{\mathrm{T}}, q_{\mathrm{T}}]\right\}\right|^2$ is the target peak power and is evaluated as the square modulus of a target-only range-Doppler map $z^{(T)}[l_{\mathrm{T}}, q_T]$ at the target's range bin l_T and Doppler bin q_T;
- $P_C = E\left\{\left|z^{(C)}[l,q]\right|^2\right\}$ is the output clutter power level and is evaluated as the variance of the zero-mean clutter-only range-Doppler map $z^{(C)}[l,q]$;
- $P_N = E\left\{\left|z^{(N)}[l,q]\right|^2\right\}$ is the output noise power level.

Correspondingly:

- $SNR = P_T/P_N$ and $CNR = P_C/P_N$ are the signal-to-noise and clutter-to-noise power ratios at the output of the signal processing scheme.

The overall loss with respect to the maximum attainable SCNR can be defined as:

$$\Delta_{SCNR} = \frac{SCNR_{max}}{SCNR} \tag{9}$$

The $SCNR_{max}$ is obtained by assuming a perfect clutter suppression, i.e., $P_C = 0$, together with a perfect target

Table I: Theoretical expressions for the performance metrics for MF, RF and TRF.

Filter	ρ_{RC}	CNR
MF + OFDM fragmentation	1	$2\left(\frac{1}{M_C}\sum_{m=0}^{M_C-1}\lvert c_m\rvert^4 - 1\right) CNR_{in} \cdot \sin^2\left(\pi K \frac{q}{M}\right)$
RF + OFDM fragmentation	$\frac{1}{M_C}\sum_{m=0}^{M_C-1}\frac{1}{\lvert c_m\rvert^2}$	0
MF + non-OFDM fragmentation	1	$2\,CNR_{in} \cdot \sin^2\left(\pi K \frac{q}{M}\right)$
RF + non-OFDM fragmentation	$+\infty$	0
TRF-Z + non-OFDM fragmentation	$\frac{E_1(t)}{e^{-2t}}$	$2\,CNR_{in}\frac{[e^{-t} - e^{-2t}]}{E_1(t)} \cdot \sin^2\left(\pi K \frac{q}{M}\right)$
TRF-M + non-OFDM fragmentation	$\frac{1 - e^{-t} + E_1(t)}{\left[e^{-t} - \sqrt{t}e^{-t} + \sqrt{\frac{\pi}{4}}erf\left(\sqrt{t}\right)\right]^2}$	$2\,CNR_{in}\frac{2Ke^{-t} + 1 - te^{-t} - e^{-2t} - \left[\sqrt{t}e^{-t} - \sqrt{\frac{\pi}{4}}erf\left(\sqrt{t}\right)\right]^2}{(1 - e^{-t}) + E_1(t)} \cdot \sin^2\left(\pi K \frac{q}{M}\right)$
TRF-S + non-OFDM fragmentation	$\frac{1 - e^{-t} + t \cdot E_1(t)}{\frac{\pi}{4}erf^2\left(\sqrt{t}\right)}$	$2\,CNR_{in}\frac{1 - e^{-t} - \frac{\pi}{4}\mathrm{erf}^2\left(\sqrt{t}\right)}{(1 - e^{-t}) + tE_1(t)}\sin^2\left(\pi K \frac{q}{M}\right)$

energy focusing as that provided by the ideal CAF. Consequently $SCNR_{max} = SNR_{max} = SNR_{in}\,N$ and the SCNR loss is rewritten as:

$$\Delta_{SCNR} = \Delta_{SNR}\,(CNR + 1) \tag{10}$$

For the OFDM-fragmented case, the output CNR can be theoretically evaluated following the approach in [19] for the case of a stationary platform and a homogeneous clutter distribution across range, which yields:

$$CNR = \begin{cases} 2(\mu - 1)CNR_{in}\sin^2\left(\pi K\frac{q}{M}\right), & MF \\ 0, & RF \end{cases}, \tag{11}$$

where CNR_{in} is the input clutter-to-noise ratio, q denotes the Doppler bin index, and $\mu = \frac{1}{M_C}\sum_{m=0}^{M_C-1}|c_m|^4$ is a scale factor depending on the modulation constellation, with values $\mu = 1$ for QPSK, $\mu = 1.32$ for 16-QAM, and $\mu = 1.38\,dB$ for 64-QAM. As is apparent, the result of the MF coincides with that of the RF only for a QPSK modulation: in that case the signal power spectrum at each batch is constant, independently of the data content, and a perfect cancellation is achieved. In contrast, for larger constellations, the MF yields clutter residuals at the output of the cancellation stage. Such residuals span across the range-Doppler map following a squared sinusoidal law along the Doppler frequency $f_D = \frac{q}{N}f_s$.

The results in (11) have been generalized in Appendix A for non-OFDM signal fragments by exploiting the exponential approximation for the waveform power spectrum at each batch:

$$CNR = \begin{cases} 2CNR_{in}\sin^2\left(\pi K\frac{q}{M}\right), & MF \\ 0, & RF \end{cases} \tag{12}$$

From equation (12), we note that, operating with the MF over non-OFDM-fragmented batches, one obtains a non-zero residual clutter output power, and this is larger than that provided by (11) with typical constellation sizes. In contrast, the RF always achieves perfect clutter suppression, being able to equalize the variability associated to the transmitted data; however, in this case, this is paid in terms of a large SNR loss caused by the noise boosting.

Appendix A also details the mathematical developments required to evaluate the output CNR when the TRF techniques are employed for range compression. The result is reported in equation (13) as a function of a generic α in (6) so that it is representative of any supervision strategy. This expression is then specified in Table I for the different supervision strategies presented in [23] (see third column). As expected, all the TRFs yield a non-zero CNR at the output of the cancellation stage, since the supervision undermines the RF's capability to equalize the variability impressed by transmitted data. For the same reason, different TRF techniques have different impact on the cancellation capability. Moreover, for each technique, this impact varies with the adopted threshold.

Using the above expressions for the CNR together with the expressions for the Δ_{SNR}, all summarized in Table I, the Δ_{SCNR} can be evaluated according to (9) for different combinations of fragmentation strategies and range compression filters.

In the following, these theoretical expressions of the performance metrics are validated through simulation. Specifically, in order to better understand the output, stationary clutter returns are generated only from the first range cell with an input CNR of $CNR_{in} = 0dB$. The clutter output power is then evaluated at the target Doppler bin by averaging across all the range bins.

In Figure 3 and Figure 4 we report the results in terms of CNR and Δ_{SCNR} obtained at $f_D = 100\,Hz$ as a function of t for several range compression filters and fragmentation strategies. Clearly, the performance of both MF and RF are

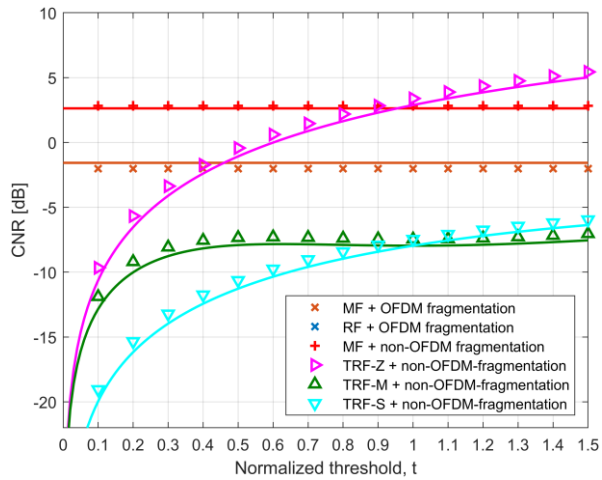

Figure 3: Output CNR obtained using MF, RF and TRF as a function of the normalized threshold t, considering both OFDM-fragmentation and arbitrarily fragmentation strategies.

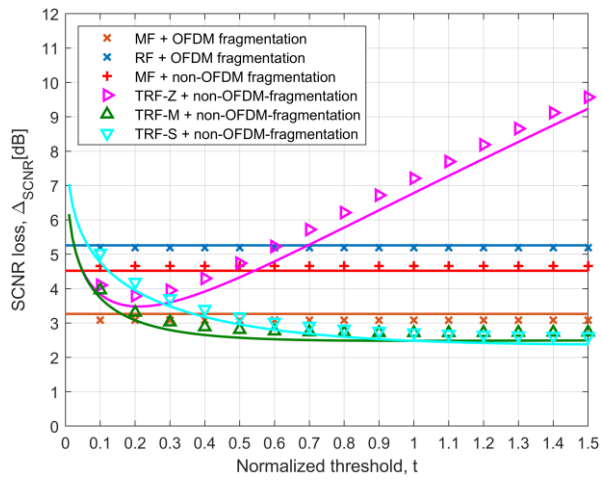

Figure 4: SCNR loss obtained using MF, RF and TRF as a function of the normalized threshold t, considering both OFDM-fragmentation and arbitrarily fragmentation strategies.

$$CNR = 2\,CNR_{in}\frac{e^{-t} - e^{-2t} + 2\alpha\sqrt{L\sigma_r^2}e^{-t}\left[\sqrt{t}e^{-t} - \sqrt{\frac{\pi}{4}}erf\left(\sqrt{t}\right)\right] + \alpha^2 L\sigma_r^2\left[1 - te^{-t} - e^{-t} - \left[\sqrt{t}e^{-t} - \sqrt{\frac{\pi}{4}}erf\left(\sqrt{t}\right)\right]^2\right]}{\left[\alpha^2 L\sigma_r^2(1 - e^{-t}) + E_1(t)\right]}\sin^2\left(\pi K\frac{q}{M}\right) \tag{13}$$

independent of the normalized threshold, so they are represented as horizontal lines. In each figure, the theoretical predictions and the simulated values are respectively represented by the solid lines and the markers.

The combinations adopting the MF exhibits an uncancelled clutter residue, namely a higher CNR, with both OFDM-fragmentation and the non-OFDM-fragmentation (Figure 3). As a consequence, despite the limited SNR loss, these solutions show a non-negligible loss in term of SCNR (see Figure 4) which increases with the input CNR, namely when the scenario is clutter limited.

The output CNR of the solutions exploiting the RF is not visible in Figure 3, since it is equal to zero ($-\infty\, dB$), yielding perfect clutter suppression as predicted by theory. Notably, this is the case not only for OFDM-fragmented signals, but also for non-OFDM-fragmented ones. However, with the RF+OFDM-fragmentation approach this advantage partially compensates for the SNR loss due to the range compression filter mismatch thus yielding a Δ_{SCNR} much comparable to the corresponding solution based on the MF (Figure 4). In contrast, with the RF + non-OFDM fragmentation approach, the Δ_{SCNR} is dominated by the SNR loss so that the improved clutter cancellation capability of the resulting scheme does not yield any practical advantage for moderate values of the CNR_{in}. For this reason, we have not included this case in the reported analysis.

The supervised TRF techniques do not achieve perfect clutter suppression, thus sensibly increasing the output CNR compared to the unsupervised RF. Yet, the residual clutter output is most often lower with the TRF than with the MF (see Figure 3). With the considered parameters, the best performing strategy is the TRF-S. As expected, the cancellation capability enabled by the TRFs degrades as the threshold increases since the impact of the data-dependent supervision becomes progressively stronger. However, it is worth observing that the CNR and the Δ_{SNR} achieved with the TRF show opposite behavior when studied as functions of the threshold (see Figure 2 and Figure 3). Therefore, the normalized threshold t could be carefully selected to obtain a good tradeoff between Δ_{SNR} and output CNR in order to achieve an improved Δ_{SCNR} with respect to other solutions (Figure 4). Note that the theoretical expressions closely match the results of the simulation, so they represent a valuable tool also for selecting an appropriate t value for the desired trade-off between SNR loss and residual CNR optimal t value.

IV. OPTIMIZED THRESHOLDED RECIPROCAL FILTER

Following the last consideration, we further observe that the theoretical expressions for Δ_{SNR}, CNR and Δ_{SCNR} also depend on the value of the parameter α, which defines different supervision techniques within the TRF family.

Based on this observation, in this section we introduce novel supervision techniques belonging to the TRF family, in which the α value is selected to maximize the adopted performance metrics: Δ_{SNR}, CNR and Δ_{SCNR}, respectively. This approach gives rise to three novel techniques:

- TRF-maxSNR: designed to minimize Δ_{SNR}
- TRF-minCNR: designed to minimize CNR
- TRF-maxSCNR: designed to minimize Δ_{SCNR}

The corresponding optimized α values are evaluated in Appendix B and reported in Table II.

Although the TRF-maxSCNR technique ideally achieves the best performance by providing the best trade-off between cancellation capability and SNR loss, its α value depends on the CNR_{in}, implying that the TRF-maxSCNR supervision technique changes depending on the clutter conditions which in turn have to be known at the receiver. Furthermore, the α value of the TRF-maxSCNR technique depends on the Doppler bin index q, which makes it impractical.

Therefore, in the following, we consider also a modified version of the TRF-maxSCNR, TRF-maxSCNRsub, where an average α value across the Doppler bins is used in lieu of the optimal one:

$$\bar{\alpha} = -\frac{[E_1(t) + CNR_{in}e^{-t}]\xi}{\sqrt{L\sigma_r^2}[(1-e^{-t}) + CNR_{in}(1-e^{-t}-te^{-t})]e^{-t}} \qquad (14)$$

By substituting the α values Table II into the equations describing the adopted performance metrics, we can verify the effectiveness of the new approaches. As in the previous sections, the theoretical formulas are also compared with the results of simulations. The results are reported in (c)

Figure 5(a)-(c) for the Δ_{SNR}, CNR and Δ_{SCNR}, respectively, using the same scenario of Figure 3 and Figure 4. The performance of the traditional MF and RF approaches are reported for comparison. Moreover, we have included the TRF-S, which exhibited the lowest SCNR loss among the TRF techniques introduced in [23].:

As discussed earlier, the theoretical curves closely match the simulated results, with limited deviations due to the adopted approximations.

The optimized TRF techniques yield further improvements compared to the previously introduced TRF ones, without any significant increase in computational complexity.

As expected, among the TRF family solutions, the TRF-maxSNR achieves the minimum SNR loss whereas the TRF-minCNR yields the best cancellation capability so that they should be considered in noise-limited and clutter-limited scenarios, respectively.

Table II: α for the optimized TRF techniques. $\xi = \left[\sqrt{t}e^{-t} - \sqrt{\frac{\pi}{4}}erf(\sqrt{t})\right]$.

Filter	α
TRF-maxSNR	$-\frac{\xi \cdot E_1(t)}{\sqrt{L\sigma_r^2}(1-e^{-t})e^{-t}}$
TRF-minCNR	$\frac{-\nu - \sqrt{\nu^2 + 4(1-e^{-t})\xi^2 e^{-2t}E_1(t)}}{2\xi\sqrt{L\sigma_r^2}(1-e^{-t})e^{-t}}$ $\nu = (1-e^{-t})^2e^{-t} - (1-te^{-t}-e^{-t}-\xi^2)E_1(t)$
TRF-maxSCNR	$-\frac{\left[E_1(t)+2\,CNR_{in}\cdot sin^2\left(\pi K\frac{q}{N_p}\right)e^{-t}\right]\xi}{\sqrt{L\sigma_r^2}\left[(1-e^{-t})+2\,CNR_{in}\cdot sin^2\left(\pi K\frac{q}{N_p}\right)(1-e^{-t}-te^{-t})\right]e^{-t}}$
TRF-maxSCNR sub	$-\frac{[E_1(t) + CNR_{in}e^{-t}]\xi}{\sqrt{L\sigma_r^2}[(1-e^{-t}) + CNR_{in}(1-e^{-t}-te^{-t})]e^{-t}}$

In intermediate scenarios, the techniques aimed at maximizing the SCNR represent the best solutions provided that a reliable estimate of the input CNR is available. Specifically, comparing the performance of the TRF-maxSCNRsub and the TRF-maxSCNR, we note that the approximation in equation (14) has a limited impact. Therefore, the sub-optimal (but cost-effective) TRF-maxSCNRsub could be preferred for a practical implementation.

V. RESULTS FOR A SIMULATED CASE STUDY

In the previous sections, the clutter suppression capabilities achieved with the TRF techniques have been assessed with reference to a single stationary scatterer at zero range and zero Doppler. This allowed us to neglect the batch processing losses ρ_{CC} and ρ_{DOP}, and to focus on the comparison between the different TRF techniques. In this section, we carry out a more realistic simulation, in which the clutter component is obtained as the superposition of the echoes from a grid of stationary scatterers, located within a 180° angular sector and spanning $N_R = 1000$ range cells, corresponding to a bistatic range of 4 km.

We consider the case study of a DVB-T-based PR for maritime surveillance and we exploit an 8k-mode DVB-T signal of opportunity, modulated using 64-QAM, with a guard interval corresponding to 1/4 of the useful symbol duration, so that $T_U = 896\mu s$ and $T_s = \left(1 + \frac{1}{4}\right) T_U = 1120\mu s$.

Figure 6 (a)-(i) show a series of range-velocity maps, each obtained using a different combination of range compression filter and fragmentation strategy. The CPI has a duration of approximately 0.57s, corresponding to $N_p = 512$ OFDM symbols, each consisting of $L = 8192$ OFDM carriers. Since the all the simulated targets are located at long ranges and move relatively slow, we conveniently used batches corresponding to $n_{sym} = 4$ OFDM symbols. For all the TRF techniques, we set the normalized threshold to $t = 0.75$. An input CNR of $CNR_{in} = 5\ dB$ has been assumed. In addition, we consider three targets of interest.

- T1: at $R_1 = 10\ km$ and moving at $v_b = 4m/s$;
- T2: at $R_2 = 50\ km$ and moving at $v_b = -8m/s$;
- T3: at $R_3 = 100\ km$ and moving at $v_b = 12m/s$;

For each target, we assumed an input SNR of $SNR_{in} = -40\ dB$ before range compression and Doppler processing.

To assess the detection performance for the three targets, we evaluate a local SCNR measure, defined as the ratio between the peak power of each target and the average interference (clutter + noise) power level within an area surrounding the target location. The results are reported in each figure with an enlarged view around the targets' position.

As is apparent, most TRFs achieve improved SCNRs compared to the MF and the RF, which clearly reveals a better target discrimination capability against the interference background. As expected, the TRF-maxSCNRsub achieves the best performance among the family of TRF supervision techniques. In this specific simulation trial, identical results are provided by the TRF-M, while the TRF-S shows only a slightly lower performance (0.1dB less against all the three targets)

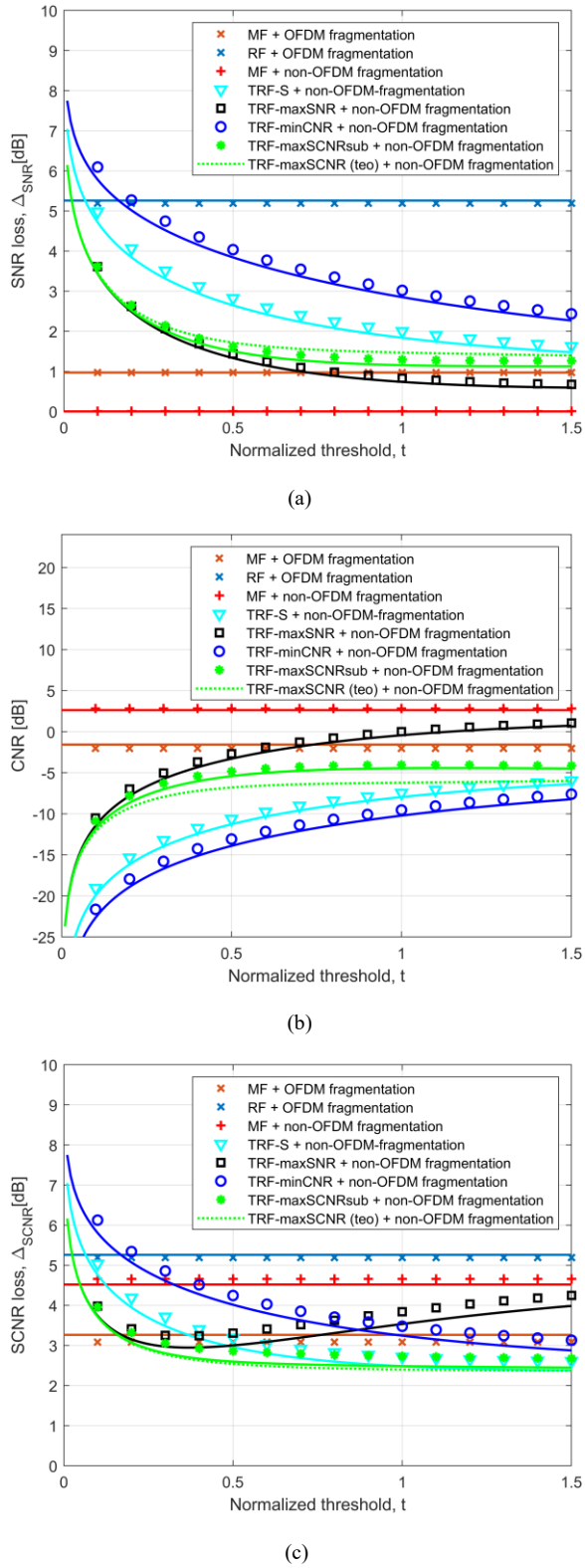

Figure 5: Performance metrics of MF, RF and optimized TRF as a function of the normalized threshold t: (a) Δ_{SNR}, (b) Output CNR, (c) Δ_{SCNR}.

To carry out a more in-depth analysis, we evaluate the local SCNR measure as a function of the input CNR, while maintaining the input SNR constant and equal to $-40dB$. The results are reported in Figure 7 for target T3, for a value of the normalized threshold of $t = 0.75$. The following observations are in order.

- The MF + OFDM fragmentation performs well at low CNR_{in} values. In fact, when the scenario is noise-limited, its performance is essentially affected by the batch processing losses ρ_{CC} and ρ_{DOP}, as well as by the loss ρ_{CP} due to the CP removal.
- Similarly, the MF + non-OFDM fragmentation achieves good detection performance in low CNR conditions. For the considered target, it outperforms the MF + OFDM-fragmentation, since it preserves the CP, thus avoiding the ρ_{CP} loss. Furthermore, it is also robust to the range-dependent loss ρ_{CC}, thanks to the increased batch duration.
- As discussed in Section II, compared to the MF + OFDM fragmentation approach, the RF + OFDM fragmentation technique experiences an SNR loss of $\zeta = 4.2901\ dB$ for 64-QAM modulated OFDM signals. However, its superior clutter cancellation capabilities renders this solution independent of CNR_{in}.
- Even though the RF + non-OFDM fragmentation strategy also achieves perfect clutter suppression, it experiences a substantial SNR loss as discussed in Section II. Consequently, its performance falls below the scale used in Figure 7.
- Such SNR loss can be prevented by using one of the TRF techniques, which in this way effectively enable the use of RF with arbitrarily fragmented OFDM signals. Particularly, they outperform the conventional MF and RF by a few dBs within the region of intermediate CNR values, i.e. $CNR_{in} = [0dB, 10dB]$. This improvement is attributed to the better trade-off between SNR loss provided at the batch processing and the cancellation capability enabled across batches. However, when the scenario is heavily clutter-limited, the RF + OFDM-fragmentation approach remains preferable, due to its superior clutter suppression capabilities.
- As expected, among the TRF techniques, the TRF-maxSCNRsub achieves the best performance. Note that the performance of the TRF-maxSCNRsub technique approaches that of the TRF-maxSNR in low CNR scenarios, and that of the TRF-minCNR in high CNR scenarios.

To understand the performance limits of the supervised approaches, in Figure 8 we revisit the analysis presented in Figure 7, optimizing the threshold value t for each input CNR using the theoretical expression for Δ_{SCNR}. To make

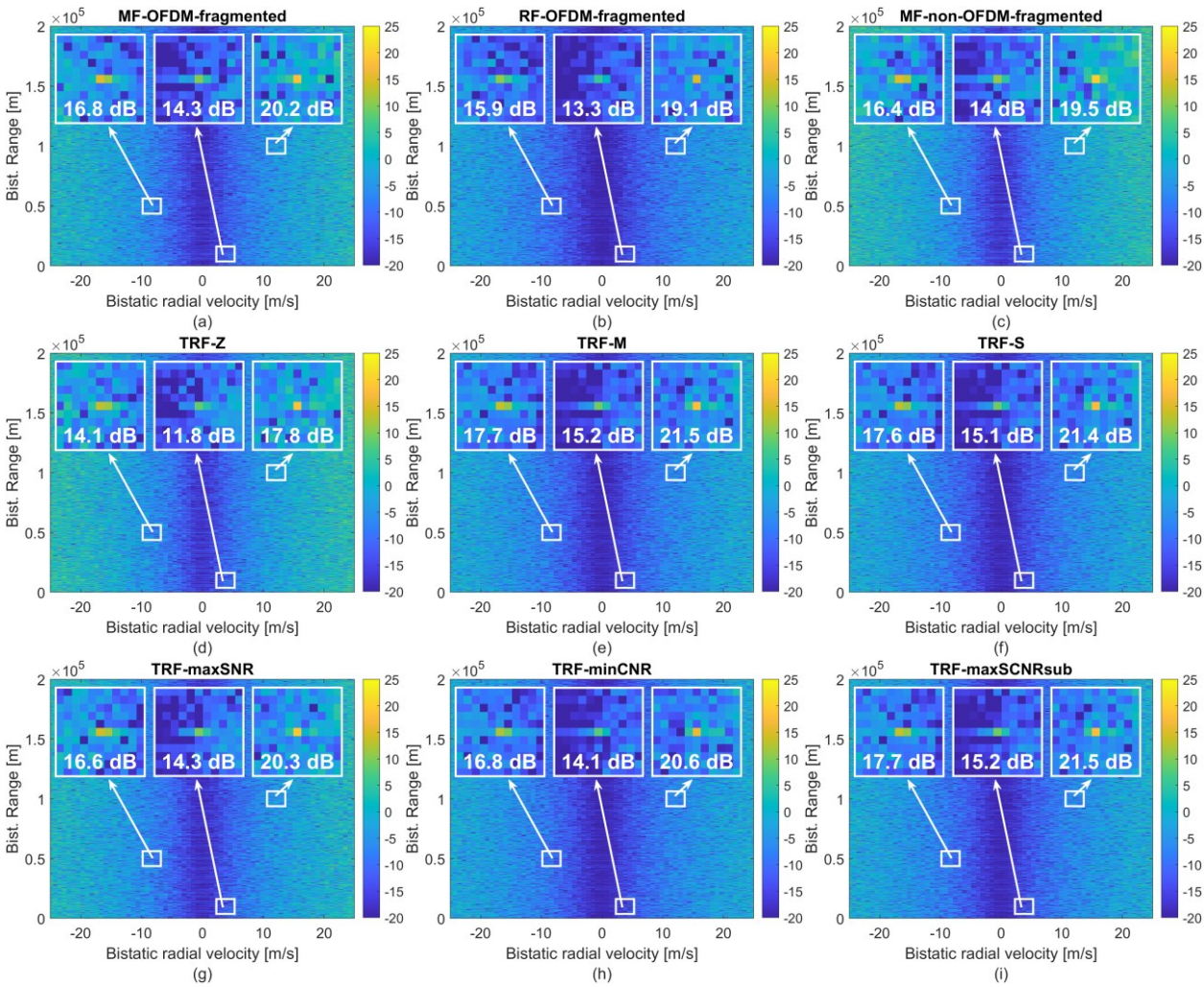

Figure 6: Output range-velocity maps obtained using (a) MF + OFDM fragmentation, (b) RF + OFDM fragmentation, (c) MF + non-OFDM fragmentation, (d) TRF-Z, (e) TRF-M, (f) TRF-S, (g) TRF-maxSNR, (h) TRF-minCNR, (i) TRF-maxSCNR. An input CNR of $CNR_{in} = 5dB$ has been assumed.

the optimal threshold independent of the target's Doppler bin q, we conduct a min-max optimization, by replacing the Doppler-dependent term $\sin^2(\pi Kq/M)$ with its maximum value. Hence, we look for the threshold t that minimizes the following expression:

$$\hat{\Delta}_{SCNR} = \frac{\alpha^2 L\sigma_r^2(1-e^{-t}) + E_1(t)}{\left[e^{-t} - \alpha\sqrt{L\sigma_r^2}\left[\sqrt{t}e^{-t} - \sqrt{\frac{\pi}{4}}erf(\sqrt{t})\right]\right]^2}\left(\widehat{CNR}+1\right), \quad (15)$$

where

$$\widehat{CNR} = 2\,CNR_{in}\frac{[e^{-t}-e^{-2t}]+2\alpha\sqrt{L\sigma_r^2}\xi e^{-t}+\alpha^2 L\sigma_r^2[1-te^{-t}-e^{-t}-\xi^2]}{[\alpha^2 L\sigma_r^2(1-e^{-t})+E_1(t)]}. \quad (16)$$

As visible by comparing Figure 7 and Figure 8, when an optimized threshold t is used, the improvement of the TRF techniques over conventional MF and RF-based approaches becomes even more pronounced. This further demonstrates the advantages deriving from the availability of a theoretical prediction for the performance metrics. Anyway, the above considerations in terms of comparative analysis among different range compression strategies still apply though over slightly modified CNR regions.

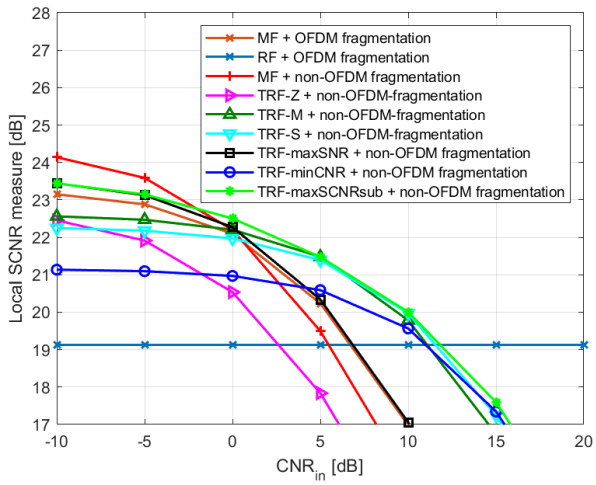

Figure 7: Local SCNR measure obtained using MF, RF and TRF, as a function of the input CNR. A normalized threshold $t = 0.75$ has been used.

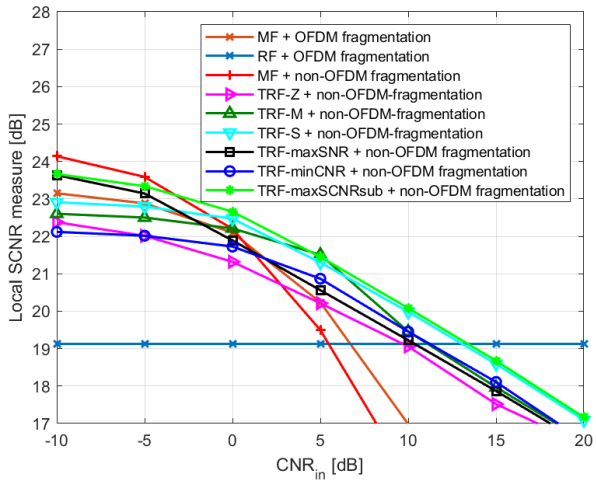

Figure 8: Local SCNR measure obtained using MF, RF and TRF, as a function of the input CNR. For each TRF technique and each CNR_{in} value, the normalized threshold t has been optimized based on (15).

VI. EXPERIMENTAL RESULTS

The TRF techniques have also been tested against an experimental dataset, collected along the shore of Civitavecchia (Italy) by exploiting a DVB-T-based receiver from the Radar and Remote Sensing Group at Sapienza University.

The acquisition geometry is shown in Figure 9 while the main parameters of the adopted waveform are reported in Table III. Specifically, an 8k DVB-T signal of opportunity was parasitically exploited to detect several maritime targets, including non-cooperative ships and the small cooperative boat shown in Figure 10. The DVB-T transmitter is located at $\approx 4400m$ from the receiver, and the reference signal is obtained by exploiting a dedicated antenna.

Table III. Parameters of the experimental test.

Symbol	Description	Value
DVB-T signal parameters		
f_c	Carrier frequency	690 MHz
T_S	OFDM symbol duration	1100 us
T_U	Useful part duration	896 us
T_{CP}	CP duration	112 us
C	Constellation	64QAM
Processing parameters		
T_{CPI}	Coherent Processing Interval duration	0.57 s

Six maritime targets of interest, denoted as T1-T6, are present in the observed scene. Specifically, T4 is the small cooperative boat shown in Figure 10, while T5 is the sailing boat in Figure 11.

As for the simulated scenario, the processing scheme in Figure 1 was employed to evaluate the range-velocity map. The SC delay was set to $K = 15$ OFDM symbols. All the different combinations of range compression filters and fragmentation strategies have been tested. In the non-OFDM fragmentation cases, we used a batch duration of length corresponding to $n_{sym} = 1.5$ OFDM symbols rather than $n_{sym} = 4$, since the targets in this case are not so far in range.

Figure 9 Setup for the experimental data acquisition.

Figure 10 Small cooperative boat (target T4).

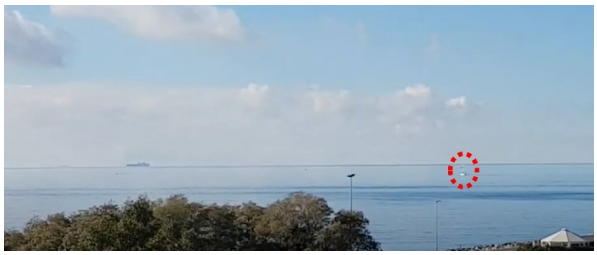

Figure 11 – Sailing boat (target T5).

Figure 12 (a)-(d) shows the output range-velocity maps obtained using MF, RF, TRF-S and TRF-maxSCNRsub, all with a non-OFDM fragmentation strategy. Here, the six targets are identified by the white boxes.

To assess the detection performance achieved using the different approaches, for each target we evaluate a local SCNR measure as the ratio between the peak amplitude and the mean level of residual disturbance, evaluated by averaging over an area of 20×20 pixels symmetrical in Doppler to the target location, namely centered in $[R_i, -v_i]$ in order to avoid the target's sidelobes influence. The local SCNR measures obtained for the six targets of interest are reported in Table IV. Here, we also included the SCNR measures achieved using both MF and RF + OFDM fragmentation approaches, as well as the SCNR measures obtained using each of the supervision techniques within the TRF family.

The following observations are in order:

- Even though the MF-based approaches achieve the lowest SNR loss, the poor clutter cancellation performance degrades the local SCNR measure for all the considered targets, both with OFDM fragmentation and non-OFDM fragmentation. The uncancelled clutter residue is also visible in Figure 12 (a) for the approach based on MF + non-OFDM fragmentation.
- The RF-based approaches have been demonstrated to guarantee the highest cancellation capability. However, they suffer from high SNR losses, especially when applied on non-OFDM signal batches The RF + non-OFDM fragmentation approach (Figure 12 (b)) undergoes an extremely high SNR loss, sensibly degrading the local SCNR measure on T1-T6, as visible in Table IV. Conversely, the RF + OFDM fragmentation approach provides a high SCNR for the fast-moving targets (namely T2 and T4), since the loss ρ_{DOP} dominates over ρ_{CC} and a shorter batch duration is preferred. However, it also shows sensible losses against the other targets (e.g. T6), depending on their radar cross section and their location in the range-velocity plane.
- As discussed in the previous sections, the TRF are designed to mitigate the SNR loss of the unsupervised RF. This is achieved at the expenses of a higher uncancelled clutter residue compared to the

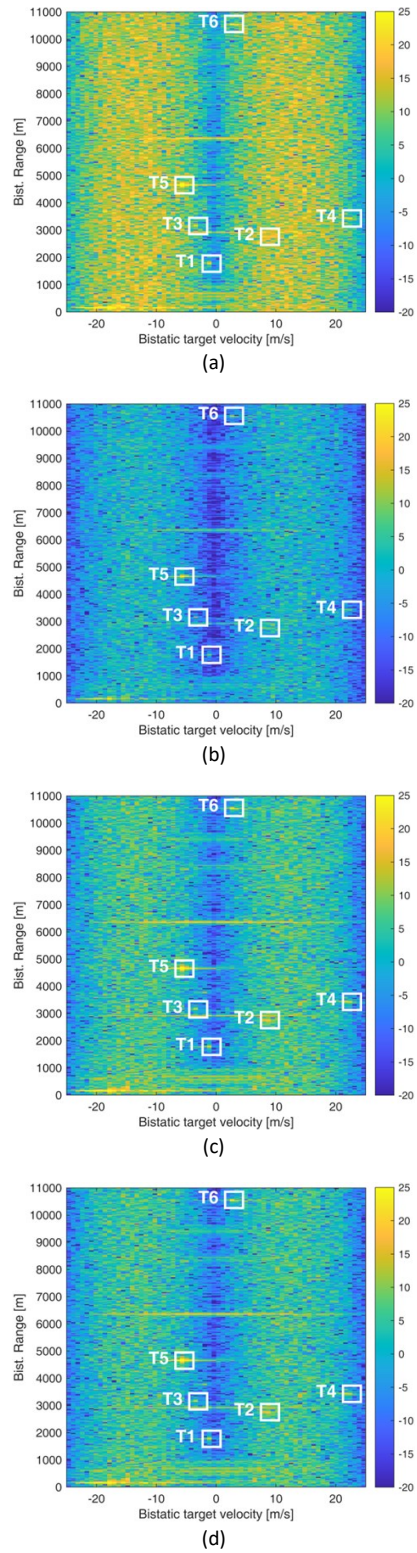

Figure 12 – Output range-velocity maps obtained on experimental DVB-T based passive radar data with (a) MF (b) RF (c) TRF-S (d) TRF-maxSCNRsub and a non-OFDM fragmentation strategy at the range compression stage, followed by a SC based clutter cancellation.

Table IV. Local SCNR measure using the different processing schemes.

Scheme	T1	T2	T3	T4	T5	T6
MF + OFDM fragmentation	11,1 dB	12,3 dB	11,4 dB	14,1 dB	22,4 dB	16,5 dB
RF + OFDM fragmentation	13,9 dB	15,9 dB	14,1 dB	16,7 dB	23,9 dB	18,9 dB
MF + non-OFDM fragmentation	**8,2 dB**	**9,5 dB**	**8,9 dB**	**10,0 dB**	**21,1 dB**	**15,6 dB**
RF + non-OFDM fragmentation	**9,5 dB**	**10,8 dB**	**12,1 dB**	**10,6 dB**	**22,5 dB**	**16,5 dB**
TRF-Z + non-OFDM fragmentation	12,0 dB	11,2 dB	13,2 dB	13,1 dB	24,0 dB	18,5 dB
TRF-M + non-OFDM fragmentation	13,9 dB	13,2 dB	14,3 dB	14,8 dB	25,0 dB	20,4 dB
TRF-S + non-OFDM fragmentation	**14,4 dB**	**13,8 dB**	**14,8 dB**	**15,2 dB**	**25,3 dB**	**20,9 dB**
TRF-maxSNR + non-OFDM fragmentation	10,3 dB	10,1 dB	10,3 dB	11,5 dB	22,5 dB	17,2 dB
TRF-minCNR + non-OFDM fragmentation	14,5 dB	14,3 dB	15,1 dB	15,4 dB	25,5 dB	20,9 dB
TRF-maxSCNRsub + non-OFDM fragmentation	**14,7 dB**	**14,3 dB**	**15,1 dB**	**15,5 dB**	**25,5 dB**	**21,1 dB**

unsupervised RF. Overall, each of the TRF approaches achieves higher local SCNR measures on all the considered targets compared to the RF + non OFDM fragmentation one. Specifically, the TRF-S shown in Figure 12 (c) obtains the highest local SCNR measures among the conventional TRF approaches.

- As to the optimized TRFs, we note that the TRF-maxSCNRsub achieves the best performance within the TRF family, slightly improving the TRF-S and yielding the highest SCNR measures across most of the considered targets.

Overall, the results achieved on experimental data confirm the observations made on simulated data and anticipated by the theoretical derivations of the performance metrics. Also, they demonstrate the practical feasibility and effectiveness of the proposed approaches.

VII. CONCLUSION

Building upon the results in [23], where the TRF supervision techniques were introduced to mitigate the significant SNR loss affecting the performance of the RF + non-OFDM fragmentation approach, in this paper we studied their impact on the clutter suppression capability of the system.

Firstly, we theoretically derived the residual clutter output power obtained using the TRF techniques. Secondly, we introduced three new supervision techniques within the TRF family, namely the TRF-maxSNR, TRF-minCNR, and TRF-maxSCNRsub. For these techniques, the parameter α is optimized based on the theoretical derivation of the performance metrics, respectively: Δ_{SNR}, CNR and Δ_{SCNR}.

The obtained theoretical results have been validated through simulated analysis, confirming that TRF techniques consistently outperform traditional MF and RF methods, especially in scenarios with moderate CNR. Furthermore, we assessed the performance of the TRF techniques using an experimental dataset, showing the effectiveness of the TRF techniques against real-world scenarios.

Future research endeavors may explore the application of TRF supervision techniques in passive radar systems installed on mobile platforms, where clutter suppression presents unique challenges. In addition, based on the analysis reported in this paper, novel supervision techniques could be identified to improve the clutter suppression performance, fully restoring the RF's clutter cancellation performance.

APPENDIX A

In the following, we derive the output CNR achieved by the non-OFDM-fragmented solutions introduced in this paper. The output CNR is defined as:

$$CNR = \frac{P_C}{P_N} = \frac{E\left\{\left|z_{DPCA}^{(C)}[l,q]\right|^2\right\}}{E\left\{\left|z_{DPCA}^{(N)}[l,q]\right|^2\right\}} \tag{17}$$

The first step is to derive the output power of the clutter and noise components, separately. To this end, we let $z^{(C)}[l,q]$ and $z^{(N)}[l,q]$ denote respectively the clutter-only and the noise-only output range-Doppler maps.

The noise output power is obtained by evaluating the expected value of the absolute square of the noise-only range-Doppler map $z^{(N)}[l,q]$:

$$P_N = E\left\{\left|\frac{1}{L}\sum_{m=0}^{M-1} e^{-\frac{j2\pi mq}{M}} \sum_{p=0}^{L-1} X_{SC}^{(N)}[p,m] e^{\frac{j2\pi pl}{L}}\right|^2\right\}, \tag{18}$$

$X_{SC}^{(N)}[p,m]$ being the DFT of the signal at the output of the SC:

$$X_{SC}^{(N)}[p,m] = S^{(N)}[p,m]H[p,m] - S^{(N)}[p,m-K]H[p,m-K] \tag{19}$$

where $S^{(N)}[p,m]$ denotes the DFT transformed noise component in the surveillance signal.

Now it is easy to verify that

$$E\left\{X_{SC}^{(N)}[p,m]X_{SC}^{*(N)}[p',m']\right\} = \\ = \begin{cases} 0, & if\ m \neq m'\ or\ \ p \neq p' \\ L\sigma_N^2 E\{|H[p,m]|^2\} + L\sigma_N^2 E\{|H[p,m-K]|^2\}, & otherwise \end{cases} \tag{20}$$

Therefore, the output noise power becomes:

$$P_N = \frac{L\sigma_N^2}{L^2}\sum_{m=0}^{M-1}\sum_{p=0}^{L-1} E\{|H[p,m]|^2\} + E\{|H[p,m-K]|^2\} = \\ = \sigma_N^2 M[E\{|H[p,m]|^2\} + E\{|H[p,m-K]|^2\}] \tag{21}$$

Similarly, the clutter output power is obtained by evaluating the expected value of the absolute square of the clutter-only range-Doppler map $z^{(C)}[l,q]$:

$$P_C = E\left\{\left|\frac{1}{L}\sum_{m=0}^{M-1} e^{-\frac{j2\pi mq}{M}} \sum_{p=0}^{L-1} X_{SC}^{(C)}[p,m] e^{\frac{j2\pi pl}{L}}\right|^2\right\} \tag{22}$$

Assuming that a grid of stationary scatterers is present, located within the angular sector Θ and spanning N_R range cells, $X_{SC}^{(C)}[p,m]$ can be obtained as:

$$X_{SC}^{(C)}[p,m] = \sum_{i=1}^{N_R} \int_{\theta\in\Theta} A_i(\theta)\, e^{-\frac{j2\pi p l_i}{L}} e^{\frac{j2\pi mq}{M}} \cdot \cdot \Big[|R[p,m]||H[p,m]| - |R[p,m-K]||H[p,m-K]| e^{-\frac{j2\pi Kq}{M}} \Big] d\theta \quad (23)$$

Therefore, we can write

$$E\left\{X_{SC}^{(C)}[p,m] X^{*(C)}_{SC}[p',m']\right\} = = E\left\{ \sum_{i=1}^{N_R}\sum_{i'=1}^{N_R} \int_{\theta\in\Theta}\int_{\theta'\in\Theta} A_i(\theta) A_{i'}^{*}(\theta')\, e^{-\frac{j2\pi p l_i}{L}} e^{\frac{j2\pi p' l_{i'}}{L}} e^{\frac{j2\pi mq}{M}} e^{\frac{j2\pi m' q}{M}} \cdot \cdot \left[|R[p,m]||H[p,m]| - \underset{s}{|R[p,m-K]||H[p,m-K]|} \right] \cdot \cdot \left[|R[p',m']||H[p',m']| - \underset{s}{|R[p',m'-K]||H[p',m'-K]|} \right] \right. \quad (24)$$

Since

$$E\{A_i(\theta) A_{i'}^{*}(\theta')\} = \begin{cases} \sigma_C^2, & i = i' \text{and } \theta = \theta' \\ 0, & otherwise \end{cases} \quad (25)$$

the above expression can be simplified as:

$$\left\{X_{SC}^{(C)}[p,m] X^{*(C)}_{SC}[p',m']\right\} = = 2\pi\sigma_C^2 \sum_{i=1}^{N_R} e^{-\frac{j2\pi(p-p')l_i}{L}} e^{\frac{j2\pi(m-m')q}{M}} \cdot \gamma \quad (26)$$

where γ

$$\begin{aligned}\gamma = {} & E\{|R[p,m]||H[p,m]||R[p',m']||H[p',m']|\} \\ & -E\{|R[p,m]||H[p,m]||R[p',m'-K]||H[p',m'-K]|\} \\ & -E\{|R[p,m-K]||H[p,m-K]||R[p',m']||H[p',m']|\} \\ & +E\{|R[p,m-K]||H[p,m-K]||R[p',m'-K]||H[p',m'-K]|\}\end{aligned} \quad (27)$$

By defining

$$\begin{aligned}\rho &= E\{|R[p,m]|^2 |H[p,m]|^2\} \\ \mu &= E\{|R[p,m]||H[p,m]|\}\end{aligned} \quad (28)$$

the expected value γ can be specified in the following cases

- $m = m'$ and $p = p'$

$$\gamma = \rho - \mu^2 - \mu^2 + \rho = 2\rho - 2\mu^2 \quad (29)$$

- $m = m' - K$ and $p = p'$

$$\gamma = \mu^2 - \rho - \mu^2 + \mu^2 = -\rho + \mu^2 \quad (30)$$

- $m = m' + K$ and $p = p'$

$$\gamma = \mu^2 - \mu^2 - \rho + \mu^2 = -\rho + \mu^2 \quad (31)$$

- *all the other cases*

$$\gamma = \mu^2 - \mu^2 - \mu^2 + \mu^2 = 0 \quad (32)$$

With these positions, eq. (22) becomes

$$P_C = 4\frac{2\pi\sigma_C^2}{L} M N_R (\rho - \mu^2) \sin^2\left[\pi K \frac{q}{M}\right] \quad (33)$$

Having derived the output power levels P_C and P_N, the output CNR is evaluated as:

$$CNR = 4\, CNR_{in} \frac{(\rho - \mu^2)}{L\sigma_r^2[E\{|H[p,m]|^2\} + E\{|H[p,m-K]|^2\}]} \sin^2\left[\pi K \frac{q}{M}\right] \quad (34)$$

In the following, the expression above is specified for different range compression filters by evaluating the corresponding ρ and μ in (28).

- MF: $H[p,m] = R^*[p,m]$

$$\mu = E\{|R[p,m]||H[p,m]|\} = E\{|R[p,m]|^2\} = L\sigma_r^2 \quad (35)$$

$$\rho = E\{|R[p,m]|^2 |H[p,m]|^2\} = E\{|R[p,m]|^4\} = 2L^2\sigma_r^2 \quad (36)$$

$$(\rho - \mu^2) = L^2\sigma_r^4 \quad (37)$$

Furthermore,

$$L\sigma_r^2[E\{|H[p,m]|^2\} + E\{|H[p,m-K]|^2\}] = 2L^2\sigma_r^4 \quad (38)$$

Therefore:

$$CNR = 2\, CNR_{in} \sin^2\left[\pi K \frac{q}{M}\right] \quad (39)$$

- RF: $H[p,m] = 1/R[p,m]$

$$\mu = E\{|R[p,m]||H[p,m]|\} = 1 \quad (40)$$

$$\rho = E\{|R[p,m]|^2 |H[p,m]|^2\} = 1 \quad (41)$$

$$(\rho - \mu^2) = 0 \quad (42)$$

Therefore:

$$CNR = \frac{P_C}{P_N} = 0 \quad (43)$$

- TRF: $H[p,m] = \begin{cases} \frac{1}{R[p,m]}, & if |R[p,m]|^2 > x_0 \\ \alpha \cdot e^{j\angle R[p,m]}, & if\ |R[p,m]|^2 \le x_0 \end{cases}$

$$\begin{aligned}\mu = {} & E\{|R[p,m]||H[p,m]|\} = \\ & = \int_0^{x_0} \sqrt{x}\alpha \frac{1}{L\sigma_r^2} e^{-\frac{x}{L\sigma_r^2}} dx + \int_{x_0}^{\infty} \frac{1}{L\sigma_r^2} e^{-\frac{x}{L\sigma_r^2}} dx \\ & = e^{-t} - \alpha\sqrt{L\sigma_r^2}\xi\end{aligned} \quad (44)$$

$$\begin{aligned}\rho = {} & \{|R[p,m]|^2 |H[p,m]|^2\} = \\ & = \alpha^2 \int_0^{x_0} x \frac{1}{L\sigma_r^2} e^{-\frac{x}{L\sigma_r^2}} dx + \int_{x_0}^{\infty} \frac{1}{L\sigma_r^2} e^{-\frac{x}{L\sigma_r^2}} dx = \\ & = \alpha^2(L\sigma_r^2 - x_0 e^{-t} - L\sigma_r^2 e^{-t}) + e^{-t}\end{aligned} \quad (45)$$

$$\begin{aligned}(\rho - \mu^2) = {} & \\ & = [e^{-t} - e^{-2t}] + 2\alpha\sqrt{L\sigma_r^2}\xi e^{-t} \\ & +\alpha^2 L\sigma_r^2[1 - te^{-t} - e^{-t} - \xi^2]\end{aligned} \quad (46)$$

where $\xi = \left[\sqrt{t}e^{-t} - \sqrt{\frac{\pi}{4}} erf\left(\sqrt{t}\right)\right]$ and $t = \frac{x_0}{L\sigma_r^2}$.

Furthermore,

$$\begin{aligned}L\sigma_r^2[E\{|H[p,m]|^2\} + E\{|H[p,m-K]|^2\}] = \\ = 2[\alpha^2 L\sigma_r^2(1 - e^{-t}) + E_1(t)]\end{aligned} \quad (47)$$

Therefore:

$$CNR = 2\, CNR_{in} \sin^2\left[\pi K \frac{q}{M}\right] \cdot \cdot \frac{[e^{-t} - e^{-2t}] + 2\alpha\sqrt{L\sigma_r^2}\xi e^{-t} + \alpha^2 L\sigma_r^2[1 - te^{-t} - e^{-t} - \xi^2]}{[\alpha^2 L\sigma_r^2(1 - e^{-t}) + E_1(t)]} \quad (48)$$

APPENDIX B

In the following, we derive the α values for the TRF-maxSNR, TRF-minCNR and TRF-maxSCNR techniques optimized according to the defined performance metrics.

TRF-maxSNR: For the TRF-maxSNR technique, we write:

$$\alpha_{TRF-maxSNR} = \underset{\alpha}{\operatorname{argmin}} \left[\frac{\alpha^2 L\sigma_r^2(1 - e^{-t}) + E_1(t)}{\left[e^{-t} - \alpha\sqrt{L\sigma_r^2}\xi\right]^2 sin^2\left(\pi K \frac{q_T}{M}\right)} \right] \quad (49)$$

since, from [23], we have

$$\Delta_{SNR} = \frac{\alpha^2 L\sigma_r^2(1-e^{-t}) + E_1(t)}{\left[e^{-t} - \alpha\sqrt{L\sigma_r^2}\xi\right]^2 sin^2\left(\pi K \frac{q_T}{M}\right)} \quad (50)$$

Deriving the expression in (50), we can find the α value which provides the minimum SNR loss:

$$\alpha_{TRF-maxSNR} = \frac{E_1(t)\left(\sqrt{\frac{\pi}{4}}erf\left(\sqrt{t}\right) - \sqrt{t}e^{-t}\right)}{\sqrt{L\sigma_r^2}(1-e^{-t})e^{-t}} \quad (51)$$

TRF-minCNR: For the TRF-minCNR technique, from equation (48) we have:

$$\alpha_{TRF-minCNR} = \\ = 2\,CNR_{in}\sin^2\left[\pi K\frac{q}{M}\right]\cdot \\ \cdot \underset{\alpha}{\operatorname{argmin}}\left[\frac{[e^{-t}-e^{-2t}] + 2\alpha\sqrt{L\sigma_r^2}\xi e^{-t} + \alpha^2 L\sigma_r^2[1-te^{-t}-e^{-t}-\xi^2]}{[\alpha^2 L\sigma_r^2(1-e^{-t}) + E_1(t)]}\right] \quad (52)$$

Deriving the expression in (52), we obtain

$$\alpha^2\{L\sigma_r^2(1-e^{-t})e^{-t}\xi\} + \\ \alpha\left\{\sqrt{L\sigma_r^2}[(1-e^{-t})^2e^{-t} - (1-te^{-t}-e^{-t}-\xi^2)E_1(t)]\right\} \quad (53) \\ \{-\xi e^{-t}E_1(t)\} = 0.$$

By taking the positive solution of this second-degree equation in α, we obtain the α value which provides the minimum CNR:

$$\alpha_{TRF-minCNR} = \frac{-\nu - \sqrt{\nu^2 + 4(1-e^{-t})\xi^2 e^{-2t}E_1(t)}}{2\xi\sqrt{L\sigma_r^2}(1-e^{-t})e^{-t}} \quad (54)$$

where

$$\nu = (1-e^{-t})^2e^{-t} \\ -(1-te^{-t}-e^{-t}-\xi^2)E_1(t) \quad (55)$$

- *TRF-maxSCNR:* For the TRF-maxSCNR technique, combining Δ_{SNR} and CNR through equation (9), we have:

$$\Delta_{SCNR} = \left\{\frac{\alpha^2 L\sigma_r^2(1-e^{-t}) + E_1(t)}{\left(\alpha\sqrt{L\sigma_r^2}\xi - e^{-t}\right)^2}\right. \\ \left. + \frac{2CNR_{in}\left[(e^{-t}-e^{-2t}) + 2\alpha\sqrt{L\sigma_r^2}\xi e^{-t} + \alpha^2 L\sigma_r^2(1-e^{-t}-te^{-t}-\xi^2)\right]}{\left(\alpha\sqrt{L\sigma_r^2}\xi - e^{-t}\right)^2}\right\} \cdot \\ \cdot \frac{\sin^2\left[\pi K\frac{q}{M}\right]}{\sin^2\left[\pi K\frac{q_T}{M}\right]} \quad (56)$$

As in the previous cases, we need to derive (56) with respect to α. This yields:

$$\alpha_{TRF-maxSCNR} = -\left[E_1(t) + 2\,CNR_{in} \\ \cdot sin^2\left(\pi K\frac{q}{M}\right)e^{-t}\right]\xi \quad (57)$$

$$\cdot \frac{1}{\sqrt{L\sigma_r^2}\left[(1-e^{-t}) + 2\,CNR_{in}\cdot sin^2\left(\pi K\frac{q}{M}\right)(1-e^{-t}\right.}$$

ACKNOWLEDGMENT

This work was partially supported by the European Union under the Italian National Recovery and Resilience Plan (NRRP) of NextGenerationEU, partnership on "Telecommunications of the Future" (PE00000001 – program "RESTART"), CUP B53C22004050001 - D.D. n.1549 del 11/10/2022.

REFERENCES

[1] B. Paul, A. R. Chiriyath, and D. W. Bliss, "Survey of RF communications and sensing convergence research," IEEE Access, vol. 5, pp. 252–270, 2017.

[2] F. Liu, C. Masouros, A. P. Petropulu, H. Griffiths, and L. Hanzo, "Joint radar and communication design: Applications, state-of-the-art, and the road ahead," IEEE Transactions on Communications, vol. 68, no. 6, pp. 3834–3862, 2020.

[3] Liu, Fan, Yuanhao Cui, Christos Masouros, Jie Xu, Tony Xiao Han, Yonina C. Eldar and Stefano Buzzi, "Integrated Sensing and Communications: Toward Dual-Functional Wireless Networks for 6G and Beyond," in IEEE Journal on Selected Areas in Communications, vol. 40, no. 6, pp. 1728-1767, June 2022, doi: 10.1109/JSAC.2022.3156632.

[4] A. Liu, Z. Huang, M. Li, Y. Wan, W. Li, T. Xiao Han, C. Liu, R. Du, D. Tan Kai Pin, J. Lu, Y. Shen, F. Colone and K. Chetty, "A Survey on Fundamental Limits of Integrated Sensing and Communication," in IEEE Communications Surveys & Tutorials, vol. 24, no. 2, pp. 994-1034, 2022, doi: 10.1109/COMST.2022.3149272.

[5] C. Berger, B. Demissie, J. Heckenbach, P. Willett and S. Zhou, "Signal processing for passive radar using OFDM waveforms," IEEE J. Sel. Topics Signal Process., vol. 4, no. 1, pp. 226–238, Feb. 2010.

[6] P. Lombardo and F. Colone, "Advanced processing methods for passive bistatic radar systems", In Principles of Modern Radar: Advanced Radar Techniques, W. L. Melvin and J. A. Scheer, Eds., SciTech, pp. 739–821, 2012.

[7] G. Gassier, G. Chabriel, J. Barrère, F. Briolle and C. Jauffret, "A Unifying Approach for Disturbance Cancellation and Target Detection in Passive Radar Using OFDM," in IEEE Transactions on Signal Processing, vol. 64, no. 22, pp. 5959-5971, Nov 2016.

[8] C.J. Coleman and H. Yardley, "Passive bistatic radar based on target illuminations by digital audio broadcasting," IET Radar Sonar and Navigation, vol. 2, no. 5, pp. 366–375, 2008.

[9] D. Poullin, "Passive Detection using broadcasters (DAB, DVB) with CODFM modulation', IEE Pros. Radar Sonar Navigation, vol.152, pp. 143-152, 2005.

[10] R. Saini, M. Cherniakov, "DTV signal ambiguity function analysis for radar application", IEE Proc. Radar Sonar and Navigation, vol.152, pp. 133-142, June 2005.

[11] J. Palmer, H. Harms, S. Searle and L. Davis, "DVB-T Passive Radar Signal Processing," IEEE Trans. on Signal Processing, pp. 2116-2126, April 2013.

[12] F. Colone, P. Falcone, C. Bongioanni, P. Lombardo, "WiFi-Based Passive Bistatic Radar: Data Processing Schemes and Experimental Results", IEEE Trans. on Aerospace and Electronic Systems, vol. 48, no. 2, pp. 1061-1079, April 2012.

[13] F. Colone, F. Filippini, M. Di Seglio and K. Chetty, "On the Use of Reciprocal Filter Against WiFi Packets for Passive Radar," in IEEE Transactions on Aerospace and Electronic Systems, vol. 58, no. 4, pp. 2746-2761, Aug. 2022, doi: 10.1109/TAES.2021.3138711.

[14] A. Evers and J. A. Jackson, "Analysis of an LTE waveform for radar applications," 2014 IEEE Radar Conference, pp. 200-205, 2014.

[15] S. Bartoletti, A. Conti and M. Z. Win, "Passive radar via LTE signals of opportunity," *2014 IEEE International Conference on Communications Workshops (ICC)*, pp. 181-185, 2014.

[16] P. Samczyński et al., "5G Network-Based Passive Radar," in IEEE Trans. on Geoscience and Remote Sensing, vol. 60, pp. 1-9, 2022.

[17] F. Colone, D. Langellotti and P. Lombardo, "DVB-T Signal Ambiguity Function Control for Passive Radars," in IEEE Transactions on Aerospace and Electronic Systems, vol. 50, no. 1, pp. 329-347, January 2014.

[18] M. Glende, "PCL-Signal-Processing for Sidelobe Reduction in Case of Periodical Illuminator Signals," 2006 International Radar Symposium, Krakow, Poland, pp. 1-4, 2006, doi: 10.1109/IRS.2006.4338042.

[19] P. Wojaczek, F. Colone, D. Cristallini and P. Lombardo, "Reciprocal Filter-based STAP for passive radar on moving platforms," in IEEE Transactions on Aerospace and Electronic Systems, vol. 55, no. 2, pp. 967-988, April 2019.

[20] J. Trujillo Rodriguez, G. P. Blasone, F. Colone and P. Lombardo, "Exploiting the Properties of Reciprocal Filter in Low-Complexity OFDM Radar Signal Processing Architectures," in IEEE Transactions on Aerospace and Electronic Systems, vol. 59, no. 5, pp. 6907-6922, Oct. 2023, doi: 10.1109/TAES.2023.3283489.

[21] J. Trujillo Rodriguez, Giovanni P. Blasone, Fabiola Colone, Pierfrancesco Lombardo, "A fast disturbance cancellation scheme for OFDM-based passive radar exploiting reciprocal filter", in IET Radar Sonar and Navigation, vol. 18, no. 1, pp. 56-67, 2024.

[22] W. Shrader and V. G. Hansen, "MTI Radar," in Radar Handbook, M. I. Skolnik, Third Edition, McGraw-Hill, 2008.

[23] J. Trujillo Rodriguez, F. Colone and P. Lombardo, "Supervised Reciprocal Filter for OFDM Radar Signal Processing," in IEEE Transactions on Aerospace and Electronic Systems, vol. 59, no. 4, pp. 3871-3889, Aug. 2023, doi: 10.1109/TAES.2023.3235317.

[24] A. Quirini, F. Colone, P. Lombardo, “Impact of supervised reciprocal filter on clutter cancellation in OFDM radar”, IEEE Int. Radar Conf. 2023, Sydney (Australia), November 2023.
[25] C. Moscardini, D. Petri, A. Capria, M. Conti, M. Martorella and F. Berizzi, "Batches algorithm for passive radar: a theoretical analysis," in IEEE Trans. on Aerospace and Electronic Systems, vol. 51, no. 2, pp. 1475-1487, April 2015.